J. Fluid Mech. (2006), *vol.* 560, *pp.* 437–448.
doi:10.1017/S0022112006000449 Printed in the United Kingdom

Turbulent flow in a converging channel: effect of contraction and return to isotropy

By MATTHEW L. BROWN[1]†, MEHRAN PARSHEH[2] AND CYRUS K. AIDUN[3]‡

[1]School of Chemical and Biomolecular Engineering, Georgia Institute of Technology, Atlanta, GA 30332, USA

[2]Institute of Paper Science and Technology, Georgia Institute of Technology, Atlanta, GA 30332, USA

[3]G.W. Woodruff School of Mechanical Engineering, Georgia Institute of Technology, Atlanta, GA 30332, USA

(Received 24 October 2005 and in revised form 27 February 2006)

We have studied the evolution of grid turbulence in a planar contraction by focusing on the flow at the centre symmetry plane. Measurements are carried out in water with inlet Taylor-microscale Reynolds number varying from 51 to 99. Detailed laser-Doppler anemometry measurements show that the streamwise fluctuating velocity component for contraction ratio $C < 2.5$ closely follows the decay of grid turbulence in a straight channel. Furthermore, the turbulent kinetic energy reaches a minimum value in the range of contraction ratio $1.5 < C < 2.5$. Turbulent intensity, independent of contraction angle and Reynolds number, decays exponentially. The results show that the flow reaches its peak of anisotropy at $2.5 < C < 3.5$ and then returns to a nearly fully isotropic state inside the contraction. The return to isotropy within the contraction is attributed to the rapid part of the pressure–strain correlation term in the transport equation of the Reynolds-stress anisotropy tensor.

1. Introduction

Turbulent flow in contractions occurs in many industrial processes and applications. In addition, the effect of contractions on turbulence is of importance for wind-tunnel design, general turbulence research, and turbulence modelling (e.g. Lumley & Newman 1977; Sjögren & Johansson 1998; Choi & Lumley 2001). Therefore, it is of both fundamental and industrial interest to study the effect of contractions on turbulence.

Assuming isotropic turbulence consists of cylindrical vortices randomly oriented in different directions, vortices with axis perpendicular to the flow direction produce the streamwise velocity fluctuations. Non-streamwise velocity fluctuations are generated by vortices aligned in the flow direction. In a contraction flow, vortices are stretched and aligned in the streamwise direction. Therefore, because of the conservation of angular momentum, it is expected that the intensity of the non-streamwise fluctuating velocity components increases while that of the streamwise component decreases. Applying Kelvin's circulation theorem to predict the intensity of vortices in an axisymmetric contraction, Prandtl (1933) has shown that this hypothesis is consistent.

† Present address: Procter & Gamble, Mehoopany, PA 18629, USA.
‡ Author to whom correspondence should be addressed: Cyrus.Aidun@me.gatech.edu

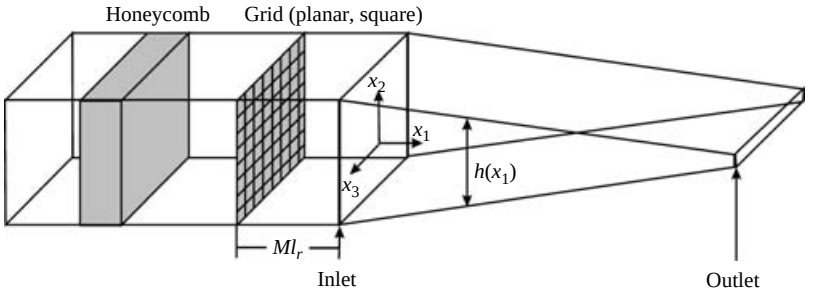

FIGURE 1. Schematic of the experimental set-up with the coordinate system.

If $U_1 + u_1$, $U_2 + u_2$ and $U_3 + u_3$ denote the instantaneous fluid velocity components (figure 1) and lower-case and capital letters denote the fluctuating and mean velocity, respectively, Prandtl's approach for axisymmetric contractions can be written as $u_1 \propto 1/C$ and $u_2, u_3 \propto \sqrt{C}$, where C denotes the contraction ratio defined as $C = U_1/U_{1,0}$, and $U_{1,0}$ being the inlet streamwise mean velocity.

The initial Taylor model (1935) has been extended by integrating over all wavenumbers (Ribner & Tucker 1953; Batchelor & Proudman 1954). In this model, the convective time scale is assumed to be much smaller than the eddy interaction time scale and, therefore, it is referred to as the 'rapid distortion theory' (RDT).

Experimental investigations of flow in axisymmetric contractions show that the rapid distortion theory correctly predicts the turbulent flow variation for contraction ratios $C < 4$ (Uberoi 1956; Hussain & Ramjee 1976). According to these studies initially isotropic turbulence becomes increasingly anisotropic up to $C = 4$ followed by a decrease in anisotropy. It is also shown that RDT significantly underpredicts the streamwise r.m.s. velocity component for $C > 4$. Tsuge (1984) found that small eddies decay through the contraction in agreement with RDT; however, large eddies are amplified due to vortex stretching.

Although some aspects of flow through axisymmetric contractions such as their influence on the velocity and thermal fluctuations (Uberoi 1956; Warhaft 1980), the effect of their shape on turbulence characteristics (Hussain & Ramjee 1976) and return to the isotropic state downstream of the outlet (Lumley & Newman 1977; Choi & Lumley 2001) have been studied, a thorough investigation of flow through planar contractions (figure 1) has not been performed thus far. Flow in channels with plane distortion (e.g. Tucker & Reynolds 1968; Gence & Mathieu 1979, 1980) cannot represent aspects of flow in planar contractions, characterized by a variable irrotational rate of strain at the centreplane. This paper aims to answer questions such as how turbulence characteristics of homogeneous turbulence vary in planar contractions and how parameters such as contraction angle, Reynolds number, inlet turbulence conditions and C, influence the development of turbulent flow in planar contractions. Experiments by Uberoi (1956) and Hussain & Ramjee (1976) revealed that inside axisymmetric contractions, the homogeneous turbulence reaches its peak of anisotropy, and then it starts to return to isotropy. Can the rapid part of the pressure–strain rate term become large enough in planar contractions so that the return to isotropy starts inside the contraction and even reaches the fully isotropic state within the contraction? In order to address these questions, we present results for turbulent flow in a planar contraction with isotropic, homogeneous grid turbulence and uniform streamwise velocity profile at the inlet. The grid position is changed relative to the inlet in order to determine the influence of the inlet turbulent intensity. The effects

Re_m	l_r	u_1' [m s^{-1}]	$u_1'/U_{1,0}$	ϵ [m^2 s^{-3}]	$R_\lambda(\equiv \overline{u_1^2}[15/(\nu\epsilon)]^{1/2})$	$R_\Lambda(\equiv u_1'\Lambda/\nu)$	η [mm]
4.5×10^3	20	0.027	0.055	0.003	51	170	0.13
9.0×10^3	20	0.053	0.054	0.012	99	636	0.10
4.5×10^3	60	0.013	0.027	1.4×10^{-4}	55	182	0.17

TABLE 1. Flow parameters at $C = 1.05$ for three selected experiments; ϵ, λ, Λ and $\eta(\equiv(\nu^3/\epsilon)^{1/4})$ denote dissipation rate, Taylor microscale, integral length scale and Kolmogorov length scale, respectively; the prime on u_1' denotes the root-mean-square value.

of contraction angle and moderate change of Reynolds number are also studied. The results are presented in terms of the development of the normal components of the anisotropy tensor and its second-moment invariant.

2. Experimental set-up

The experiments are carried out in a closed water loop. The test section is constructed of 12 mm thick Plexiglas to allow visual access. In order to introduce an isotropic homogeneous flow at the inlet, flow first passes through a hexagonal flow straightener (Honeycomb) installed in a constant-cross-section channel, figure 1. The flow straightener has an open width of 10 mm and a closed width of 0.4 mm. Free-stream turbulence is then generated by a monoplane square grid with rectangular bars. The mesh size, M, and bar width of the grid are 9.5 mm, and 3.2 mm, respectively, resulting in a solidity of 0.56. The turbulent intensity at the contraction inlet can be varied by repositioning the grid relative to the contraction inlet. This distance is normalized by M, and is denoted by l_r. In order to achieve homogenous isotropic turbulence at the contraction inlet, the grid is located at least 20 mesh sizes upstream of the contraction inlet. The contraction is 550 mm long, 155 mm wide (w) with inlet height $h_0 = 179.2$ mm (see figure 1). The contraction half-angle, β, and the maximum contraction ratio, C_{max}, are varied by changing the outlet height. The mesh Reynolds number, Re_m, is based on the mesh, M, and the mean velocity at inlet, $U_{1,0}$. By changing the flow rate, the value of Re_m is varied from 4.5×10^3 to 9.0×10^3, giving inlet velocities ranging from 0.47 to 0.94 m s^{-1}. The summary of flow parameters for three cases with $\beta = 8.4^\circ$ is presented in table 1.

A two-component LDA system (TSI) with a 5 W argon ion laser (Coherent, Innova 70) is used to measure the velocity field. Alumina particles, 0.3 μm in diameter, are used to seed the flow. The optical head is traversed automatically using a three-dimensional linear traversing system with accuracy of $\pm$0.1 mm. The LDA data are collected randomly with 5 repetitions for a period of 90 s.

3. Theoretical background

Analogous to Prandtl's (1933) approach for axisymmetric contractions, the conservation of circulation applied to a fluid element in a planar contraction (figure 1) gives $u_1' \propto 1/C$, $u_2' \propto C$, and $u_3' \propto 1$, suggesting a monotonic decrease in the streamwise r.m.s. velocity component; the prime denotes root-mean-square (r.m.s.) hereafter. However, according to the rapid distortion theory (RDT), for distortions in a planar contraction, the non-streamwise normal stress components at large C are approximated as

$$u_2', u_3' \propto \sqrt{C}, \tag{3.1}$$

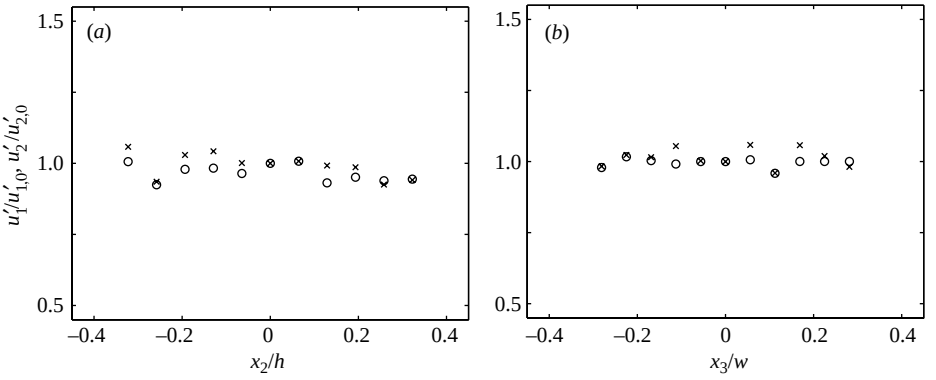

FIGURE 2. Distribution of u_1' (○) and u_2' (×) along (*a*) the x_2-axis at $x_3 = 0$ and $x_1 = 0$, (*b*) the x_3-axis at $x_2 = 0$ and $x_1 = 0$, normalized by the values at $x_1 = 0$, $x_2 = 0$ and $x_3 = 0$ for $Re_m = 4.5 \times 10^3$, $l_r = 20$; the prime on u_1' and u_2' denotes the root-mean-square value.

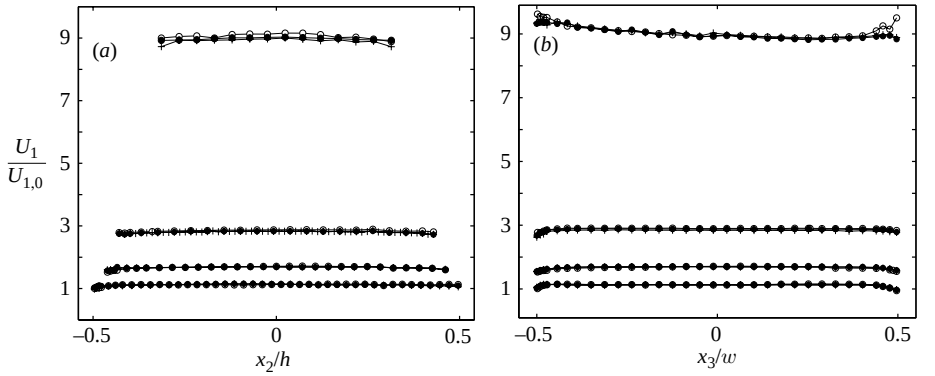

FIGURE 3. Mean streamwise velocity profile (*a*) along the x_2-axis at $x_3 = 0$, (*b*) along the x_3-axis at $x_2 = 0$ at $C = 1.2$, 1.6, 2.8 and 9.0 (bottom to top) for $Re_m = 4.5 \times 10^3$ (○), $Re_m = 6.7 \times 10^3$ (•), $Re_m = 9.0 \times 10^3$ (+).

which is similar to Prandtl's formulae for axisymmetric contractions, as stated in § 1. The prediction by RDT is more accurate since it accounts for mutual interaction of vortices.

It is important to our study to have nearly isotropic turbulence at the contraction inlet. Grid-generated turbulence tends to have slightly higher energy content in the streamwise direction. Comte-Bellot & Corrsin (1966) used an axisymmetric contraction with $C_{max} = 1.27$ to suppress the streamwise r.m.s. velocity and, therefore, to obtain perfect isotropic turbulence. Our experiments show that at the core of the contraction inlet, the difference between r.m.s. velocity components is $\pm 5\,\%$ or smaller and, thus, the turbulence is nearly isotropic. Moreover, the spatial variation in r.m.s. velocity components at $x_1 = 0$ is within $\pm 7\,\%$ as shown in figure 2, demonstrating nearly homogeneous turbulence.

The streamwise mean velocity profile along the x_2-axis at $x_3 = 0$, figure 3(*a*), and along the x_3-axis at $x_2 = 0$, figure 3(*b*), is uniform everywhere in the contraction. If the effect of the sidewalls is neglected, the contraction can be considered two-dimensional, where U_3 and $\partial(\cdots)/\partial x_3$ are negligible. The mean velocity gradient tensor, is written

as

$$\frac{\partial U_i}{\partial x_j} = \begin{pmatrix} \dfrac{\partial U_1}{\partial x_1} & \dfrac{\partial U_1}{\partial x_2} \approx 0 & \dfrac{\partial U_1}{\partial x_3} \approx 0 \\ \dfrac{\partial U_2}{\partial x_1} & -\dfrac{\partial U_1}{\partial x_1} & 0 \\ 0 & 0 & 0 \end{pmatrix}. \tag{3.2}$$

The x_1- and x_2-components of the mean vorticity vector are negligible everywhere, and the x_3-componnet, given by $\omega_3 = \partial U_2/\partial x_1$, is zero at the centreplane due to geometrical symmetry. Also, U_2 is zero at the centreplane because of symmetry.

In the following sections, the results of this study are evaluated in terms of the Reynolds-stress anisotropy tensor defined by (Lumley & Newman 1977)

$$a_{ij} = \frac{\overline{u_i u_j}}{K} - \frac{2\delta_{ij}}{3}, \tag{3.3}$$

where $K \equiv \overline{u_i u_i}/2$ is the turbulent kinetic energy.

In isotropic turbulence, all normal components of this tensor vanish identically. The transport equation for a_{ij} is given by

$$\frac{\mathrm{D}a_{ij}}{\mathrm{D}t} = \mathscr{P}_{ij} + \frac{1}{K}\left(\Pi_{ij}^{(r)} + \Pi_{ij}^{(s)}\right) - \frac{\epsilon}{K}(e_{ij} - a_{ij}) + D_{ij}, \tag{3.4}$$

where $\mathscr{P}_{ij}$ is the production of a_{ij}, and e_{ij} is the dissipation-rate anisotropy tensor defined as $e_{ij} = \epsilon_{ij}/\epsilon - 2\delta_{ij}/3$, where ϵ is the dissipation rate per unit mass. In this equation, $\mathscr{P}_{ij}$ can be obtained exactly; however, the other terms need to be modelled. Here, the diffusion term $D_{ij} = 0$ because of the homogeneity in the turbulence. The superscripts (r) and (s) denote the rapid and the slow parts of the pressure–strain rate, respectively. When the velocity gradient is large, the rapid part is the dominating term; its interplay with $\mathscr{P}_{ij}$ determines the state of isotropy. However, when the velocity gradient is zero and, thus, $\mathscr{P}_{ij} = 0$, the state of isotropy is governed by $\Pi_{ij}^{(s)}$ and e_{ij}. In general, it is difficult to directly measure the pressure–strain rate correlation (Sjögren & Johansson 1998). However, by measuring other terms in equation (3.4), this term can be computed. In § 4, we also present the data in terms of the invariants of the anisotropy tensor (Lumley 1970, 1978), given by $II = a_{ij}a_{ji}$ and $III = a_{ij}a_{jk}a_{ki}$.

4. Results

In order to quantify the effect of contraction on turbulence, we compare the evolution of grid turbulence in a contraction with reference to a straight channel. A model for decay of grid turbulence which is experimentally validated is given by $u_1'/U_{1,0} \approx 1.1\left(tU_{1,0}/M\right)^{-0.61}$ (Sirivat & Warhaft 1983; Mydlarski & Warhaft 1996) where t is time. An earlier model developed by Frenkiel (1948) and verified experimentally by Roach (1987) is based on the bar dimensions, given by

$$\frac{u_1'}{U_{1,0}} = c_\circ \left(\frac{tU_{1,0}}{d}\right)^{-5/7}, \tag{4.1}$$

where d is the bar width and $c_\circ$ is a constant based on the grid geometry and Re_m. We have compared equation (4.1) with our data. As shown in figure 4(a), this model agrees with our data up to $t \approx 32M/U_{1,0}$ (corresponding to $C \approx 2.5$) when $c_\circ = 1.13$;

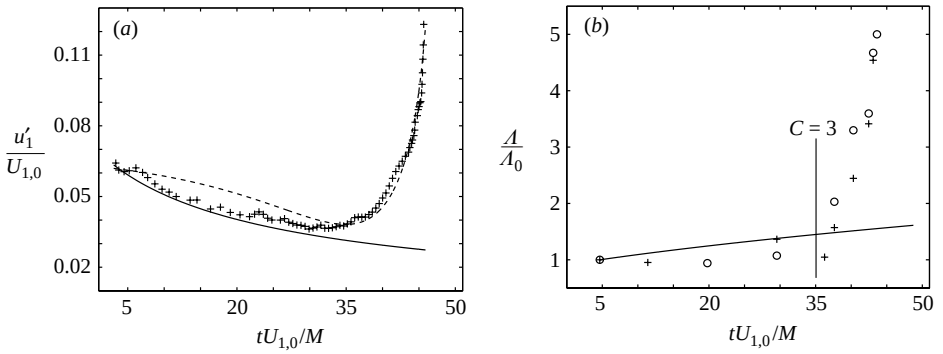

FIGURE 4. (*a*) Variation of $u_1'/U_{1,0}$ for $Re_m = 4.5 \times 10^3$ and $l_r = 20$ (+) compared to equation (4.1) (—) and based on the exponentially decaying function $e^{-1.6C^*}$ (– – –). (*b*) Integral length scale for $Re_m = 4.5 \times 10^3$ (+), $Re_m = 9.0 \times 10^3$ (○) and $\Lambda \sim t^{0.5}$ by Roach (1987) (—).

here t is time of travel measured from the inlet to the contraction at $l_r = 20$. This comparison suggests that for $C < 2.5$, the production of turbulent energy is negligible.

According to Roach (1987), the Eulerian length scale, Λ, of grid turbulence scales as $\Lambda \sim t^{0.5}$. In this study, we estimate (see Parsheh, Brown & Aidun 2005) the values of Λ in the contraction using Taylor's approximation. The variation of Λ is shown in figure 4(*b*), where Λ_0 denotes the value at $C = 1.1$. Our results are consistent with the rapid distortion theory and the results obtained by Warhaft (1980) in an axisymmetric contraction with the maximum contraction ratio of $C_{max} = 4$. In both cases, the Eulerian length scale decreases slightly up to $C \approx 3.0$ for the planar contraction (figure 4*b*), and to $C \approx 4.0$ in the axisymmetric contraction, as discussed by Warhaft. At $C > 3$, our results show a rapid increase in Λ compared to the straight channel due to the stretching of large eddies in the contraction, as predicted by Tsuge (1984).

The streamwise turbulent intensity along the centreline, $T_1 = u_1'/U_1$, for various cases with different contraction half-angle, Reynolds number and inlet turbulent intensity has been shown to decay exponentially along the contraction (Parsheh *et al.* 2005). It has also been shown that $T_1^* \equiv (T_1 - T_{1,e})/(T_{1,0} - T_{1,e})$ in all cases collapses around the same curve proportional to $e^{-1.6C^*}$, where $C^* = C - 1$ and $T_{1,0}$ and $T_{1,e}$ are the values of T_1 at inlet and outlet, respectively. This function is shown in figure 4(*a*) where it is compared to the measured results and relation (4.1).

The r.m.s. velocity components, figure 5(*a*), attain minimum values at $C \approx 2$ unlike axisymmetric contractions where the minimum occurs at $C \approx 4$ (Uberoi 1956: Hussain & Ramjee 1976; Tsuge 1984). Also, the turbulent kinetic energy has a flat minimum at $1.6 < C < 2.2$. The total uncertainty in the measured instantaneous velocity (error bars in figure 5*a*) consists of the uncertainty in the x_1-position due to the initial alignment at the origin and due to the horizontal misalignment, and the random errors associated with the LDA measurements (see for more details Brown 2005). As shown in figure 5(*a*), the position of the minimum in u_1' varies from $C \approx 2.1$ to $C \approx 1.7$ when the location of the grid is changed from $l_r = 20$ to $l_r = 60$, decreasing the inlet turbulent intensity by a factor of roughly two. This shows that the effect of the contraction on the turbulence is highly dependent on the inlet conditions, consistent with the results for axisymmetric contractions by Hussain & Ramjee (1976). This can be attributed to the negligible production of kinetic energy

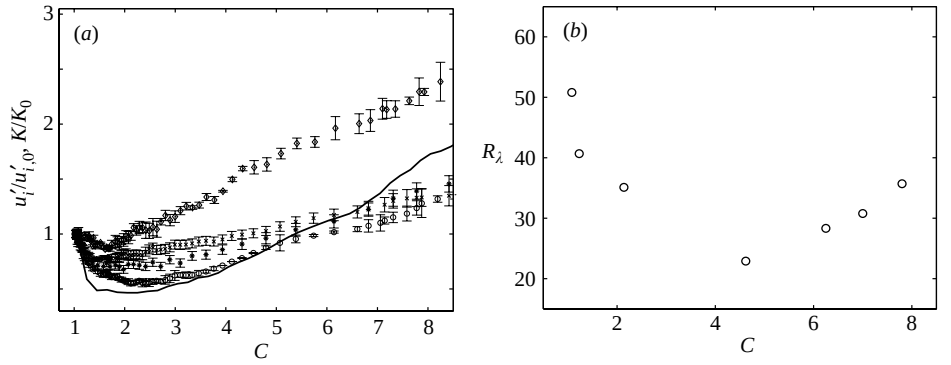

FIGURE 5. Dependence on contraction ratio. (*a*) Components of r.m.s. velocity normalized with their respective value at $x_1 = 0$; $Re_m = 4.5 \times 10^3$ and $l_r = 20$: x_1-component (o), x_2-component ($\times$), x_3-component ($*$) and K/K_0 (—); $Re_m = 4.5 \times 10^3$ and $l_r = 60$: x_1-component ($\diamond$); error bars represent 95 % confidence interval. (*b*) Reynolds number based on the Taylor-microscale $R_\lambda (\equiv \overline{u_1^2}[15/(\nu\epsilon)]^{1/2})$ with $Re_m = 4.5 \times 10^3$ and $l_r = 20$.

at $C < 2$ discussed above. Figure 5(*b*) shows the change of Reynolds number based on the Taylor-microscale Reynolds number, $R_\lambda \equiv \overline{u_1^2}[15/(\nu\epsilon)]^{1/2}$; the method by which ϵ is estimated is discussed below in this section.

The presence of a minimum value of K can be explained based on the production of turbulent kinetic energy. Considering the flow at the contraction centreline with the deformation tensor given by (3.2) with $\partial U_2/\partial x_1 = 0$ due to symmetry, the production of kinetic energy is zero in the x_3-direction, negative in the streamwise direction and positive in the x_2-direction (see Parsheh *et al.* 2005). The production of K is half the sum of the three components. Thus, for nearly isotropic turbulence at the inlet the production of energy is small, as shown and discussed above. As a result, $\mathrm{D}K/\mathrm{D}t < 0$ because of energy dissipation. Close to $C = 2$, where $\overline{u_2^2} > \overline{u_1^2}$, there is a finite production of kinetic energy given by $(\overline{u_2^2} - \overline{u_1^2})\partial U_1/\partial x_1$. At this region, the rate of dissipation reaches a minimum (as will be shown later) which is balanced by the production term and thus $\mathrm{D}K/\mathrm{D}t = 0$. From this point on, $\partial U_1/\partial x_1$ becomes large and therefore the production of energy is larger than the rate of dissipation. The increase in u_1' is most likely due to the redistribution of energy between components.

Since LDA signals are sampled randomly in time, we have used the refined sample-and-hold reconstruction method by Nobach, Müller & Tropea (1998) to estimate the power spectral density. The spectra estimated by this method have been shown to be in good agreement with the actual spectra measured by hot-wire anemometry, Nobach *et al.* (1998). The estimated one-dimensional spectra in the x_1- and x_2-directions at different contraction ratios are shown in figures 6(*a*) and 6(*b*), respectively. These spectra are shown as a function of frequency, f, and are normalized so that the area under all curves is equal to unity. Therefore, these figures show the influence of the contraction on each fluctuating scale instead of the amplitude. Consistent with the results for axisymmetric contractions (Warhaft 1980), the spectrum in the x_2-direction is not affected significantly by the contraction while the u_1-spectrum peaks at a higher frequency at larger C (Warhaft 1980 and the references therein, and the RDT by Ribner & Tucker 1952). It should be noted that the amplitude of the power spectra decreases for $C < 2.5$ in agreement with RDT and thereafter increases gradually (not shown here). The one-dimensional spectrum considered in the form of $\kappa_1 F_{11}(\kappa_1)$,

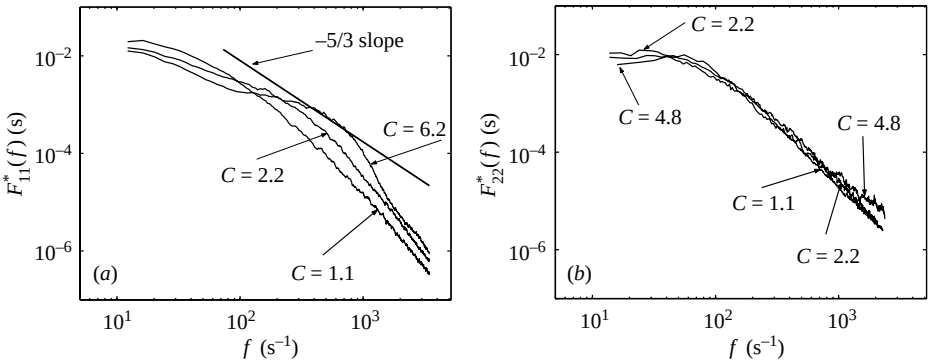

FIGURE 6. Normalized one-dimensional power spectral density in (a) the x_1-direction and (b) the x_2-direction for $Re_m = 9.0 \times 10^3$ and $l_r = 20$.

where $\kappa_1 (\equiv 2\pi f/U_1)$ is the streamwise wavenumber, has a peak, $\max(\kappa_1 F_{11})$, at κ_1^p. Our data show that the value of κ_1^p decreases with C when $C > 3.0$ and does not change significantly when $C < 3.0$. Warhaft (1980) argues that κ_1^p at $\max(\kappa_1 F_{11})$ is a measure of the integral length scale. This implies that the integral length scale should significantly increase when $C > 3.0$, which is consistent with the results shown in figure 4(b).

Measurement of energy dissipation rate, ϵ, contains some uncertainties (Burattini, Lavoie & Antonia 2005). Assuming local isotropy, ϵ can be approximated by

$$\epsilon = 15\nu \overline{\left(\frac{\partial u_1}{\partial x_1}\right)^2}. \tag{4.2}$$

In grid turbulence, Sirivat & Warhaft (1983) showed that the estimated ϵ based on equation (4.2) agrees well with the estimate from the scaling law. In grid turbulence, ϵ can be estimated directly from the decay rate of the turbulent kinetic energy, given by

$$\epsilon = -\frac{\mathrm{D}K}{\mathrm{D}t}. \tag{4.3}$$

Warhaft (1980) used equation (4.3) to estimate the dissipation rate upstream and downstream of an axisymmetric contraction with $C_{max} = 4$, in agreement with ϵ deduced from the peak of the three-dimensional energy spectrum. However, we cannot use this expression everywhere in the contraction since K increases for $C > 2$, figure 5(a). In the forced direct numerical simulation (DNS) of Alvelius (1999), it is shown that the relationship between the wavenumber at the end of the inertial subrange, κ_{inert}, and ϵ is given by

$$\epsilon \approx \frac{\nu^3}{(0.1/\kappa_{\mathrm{inert}})^4}. \tag{4.4}$$

In this study, we have used equation (4.2) to estimate the dissipation rate. However, if the flow is not fully isotropic the ϵ calculated by this method becomes inaccurate (Burattini *et al.* 2005). Therefore, in order to verify the accuracy of the calculated ϵ, we compare the results to other methods. For $C < 1.3$, we have observed that the ϵ estimated by equation (4.2) agrees with the velocity decay law estimate, equation (4.3). At $C = 2.2$, where $\mathrm{D}K/\mathrm{D}t = 0$, the value of ϵ and the production of the kinetic energy are in balance. For $C > 4.4$, ϵ calculated from (4.2) and from (4.4) are in agreement.

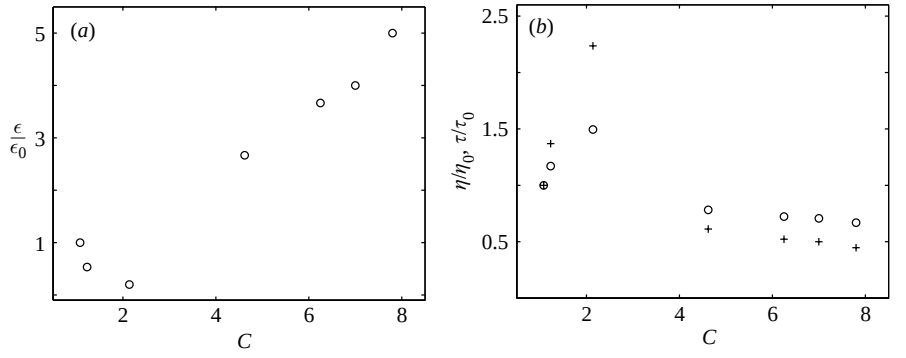

FIGURE 7. The change of (*a*) rate of dissipation per mass and (*b*) the Kolmogorov length (○) and time (+) scales normalized by their respective values at $C = 1.1$, $Re_m = 4.5 \times 10^3$ and $l_r = 20$.

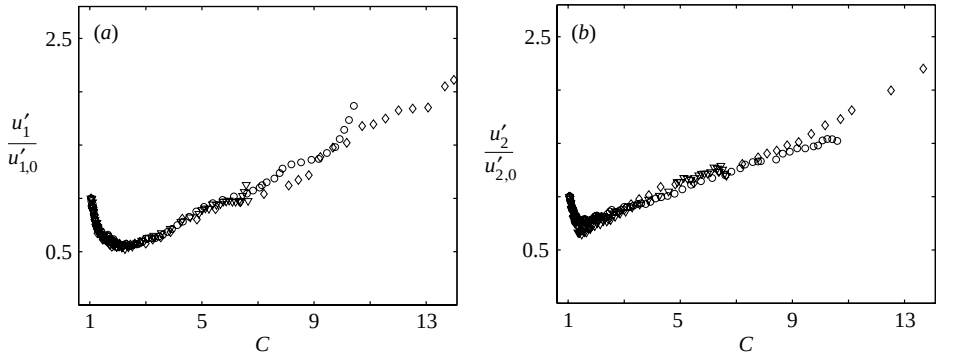

FIGURE 8. Effect of contraction angle on (*a*) x_1-component, (*b*) x_2-component of r.m.s. velocity for $\beta = 8.15°$ (▽), $\beta = 8.4°$ (○) and $\beta = 8.8°$ (◇).

Considering that for $C < 4$ a clear inertial subrange does not exist due to small R_Λ, we cannot obtain accurate values for ϵ for $2.2 < C < 4.4$. As shown in figure 7, the dissipation rate reaches a minimum (figure 7*a*) and the Kolmogorov length scale, $\eta(\equiv (\nu^3/\epsilon)^{1/4})$, and time scale, $\tau(\equiv (\nu/\epsilon)^{1/2})$, approach a maximum (figure 7*b*) at $C \approx 2$ where R_Λ is at a minimum value (this is not shown here).

According to the rapid distortion theory, contraction shape has no significant influence on the turbulence. Hussein & Ramjee (1976) verified this using four different axisymmetric contraction shapes. We study the effect of shape in planar contractions by analysing the influence of contraction angle, β, on the development of r.m.s. velocity components. This is done by varying the outlet height and keeping the grid at $l_r = 20$ and other parameters unchanged. Figures 8(*a*) and 8(*b*) show the results for contractions with $C_{max} = 7.3$, $C_{max} = 11.2$ and $C_{max} = 16.7$ with corresponding angles $\beta = 8.15°$, $\beta = 8.4°$ and $\beta = 8.8°$, respectively. Although the difference in angle, β, appears to be small, the total convective acceleration at the contraction outlet when $\beta = 8.8°$ is more than two times larger than that when $\beta = 8.15°$. As shown in figures 8(*a*) and 8(*b*) the fluctuating velocity components collapse around the same curve implying that turbulence variation with C is independent of β (the x_3-component is not shown here). Since the difference in the residence time in these cases is small, it is impossible to verify the dependence of turbulence level on residence time. The

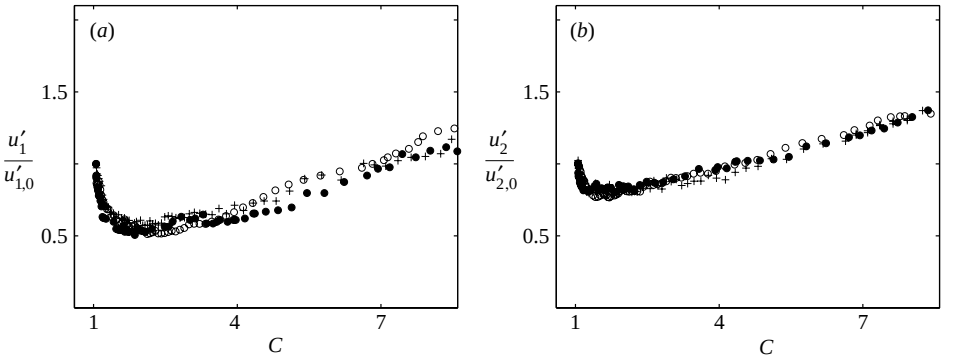

FIGURE 9. Effect of Re_m on (*a*) x_1-component, (*b*) x_2-component of r.m.s. velocity for $Re_m = 4.5 \times 10^3$ (o), $Re_m = 6.7 \times 10^3$ (•) and $Re_m = 9.0 \times 10^3$ (+).

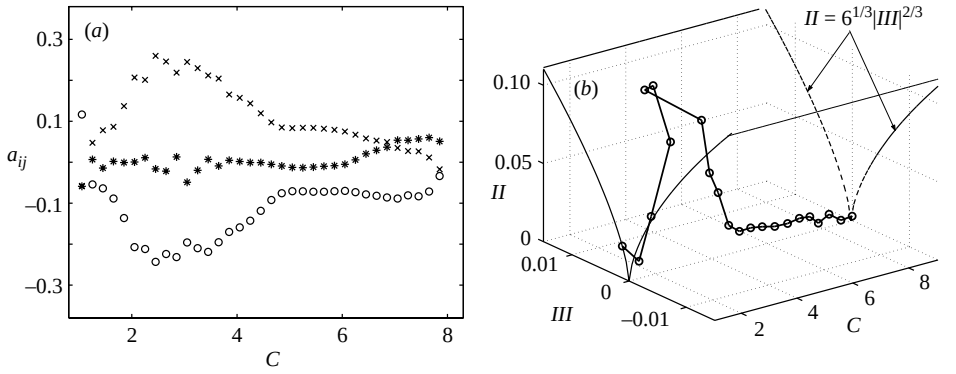

FIGURE 10. (*a*) Development of normal components of the anisotropy tensor in the contraction a_{11} (○), a_{22} (×) and a_{33} (*); (*b*) change of invariants II and III in the contraction, for $Re_m = 4.5 \times 10^3$ and $l_r = 20$.

effect of residence time should be more pronounced when Re_m is varied. This is done by changing only the flow rate and positioning the grid at $l_r = 20$. Figure 9 shows that the variation of r.m.s. velocity is nearly universal for all cases (x_3-component is not shown here). This implies that moderate changes in Re_m and, therefore, residence time do not significantly influence the turbulence in planar contractions. This is consistent with results from Ramjee & Hussain (1976) who have shown that a change of Re_m by a factor of 10 does not significantly influence the turbulence.

The tendency of returning to isotropy has been observed in various experimental investigations only when the flow is relaxed from the axial strain (e.g. by Tucker & Reynolds 1968; Gence & Mathieu 1980). Prandtl's formulae and the rapid distortion theory suggest that turbulent flow in contractions becomes highly anisotropic at large C. Our measurements show that in a planar contraction flow starts to return to the isotropic state at $C > 3.5$. According to figure 10(*a*), nearly isotropic turbulence at the inlet reaches its peak of anisotropy for $2.5 < C < 3.5$ and moves towards a fully isotropic state further downstream. Figure 10(*a*) clearly shows that a_{22} loses energy to a_{11} while the flow returns to the isotropic state. In addition, at large C the difference between a_{22} and a_{33} becomes small and within the range of the experimental error.

The return to isotropy can be partly attributed to the fact that at large C the fluctuations in the x_2- and x_3-directions are produced by the same vortices with axis

aligned in the x_1-direction as predicted by rapid distortion theory, equation (3.1) (Batchelor & Proudman 1954). According to (3.4) the balance between the rapid pressure–strain term and the production of a_{ij} determines the state of isotropy. Furthermore, figure 10(*a*) implies that at $C \approx 4$ the balance between $\mathscr{P}_{11}$, which is negative, and $\Pi_{11}^{(r)}$ turns in favour of $\Pi_{11}^{(r)}$. In the models available for $\Pi_{11}^{(r)}$ (Launder, Reece & Rodi 1975), this term is proportional to $\partial U_1/\partial x_1$, which in the planar contraction increases sharply for $C > 4$. Thus, we conclude that the large irrotational rate of strain at this region is responsible for this interesting phenomenon. In keeping with previous studies of return to isotropy, we project our results in the anisotropy invariant map, (II, III)-plane (Lumley 1978), along the contraction as shown in figure 10(*b*). The results clearly show the rapid increase of the second invariant followed by a gradual return to an almost fully isotropic state, consistent with figure 10(*a*). This view of the results shows the characteristics of the present data, compared to other turbulent flows.

5. Conclusion

The fluctuating velocity components of flow in planar contractions, in the range of convergence angles and Re_m considered in this study, go through a minimum value at $C \approx 2$. The downstream position of this minimum can be compared to that of axisymmetric contractions where the minimum occurs at $C \approx 4$. We show that the streamwise location of the minimum does not depend on the contraction angle or the Reynolds number. In general, we have shown that the Reynolds number and the contraction angle have an almost negligible influence on the variation of turbulent velocity components with C.

Turbulent intensity throughout the contraction depends significantly on the grid position and, thus, the inlet turbulence level. This is attributed to the small production of turbulent energy at $C < 2$ and large convective acceleration at $C > 2$ which offsets the production of energy. Thus, we conclude that contraction ratio and inlet turbulence level are the only parameters which significantly affect the turbulence level in the contraction.

The highly anisotropic flow starts to return to the isotropic state at $C \approx 4$ and becomes almost isotropic at $C \approx 8$. This is probably due to the redistribution of kinetic energy between different components by rapid pressure–strain rate correlation in addition to the fact that turbulent energy in the x_2- and x_3-directions is produced by the same vortices. It is important to note that the return to isotropy in planar contractions starts at $C \approx 4$, occurring much earlier than that in axisymmetric contractions.

Now, the question is whether the existing models for the rapid pressure–strain term can correctly model highly accelerating and also straining flows. Tsuge (1984) argues that when the flow has a finite spatial inhomogeneity (e.g. at large C because of increase of the size of large eddies) proposed models should consider the distribution of energy at different wavenumbers. The widely used model for the rapid pressure-correlation term by Launder *et al.* (1975) has been calibrated for different flows such as shear flow, the rapid distortion theory, and isotropic turbulence. It is obvious that models which are calibrated to homogeneous flows cannot fully simulate flows with a significant variation of eddy size, as we have shown to occur in the planar contraction. The disagreement of the streamwise component by RDT and the contraction flow confirms this conclusion. In addition, this disagreement clearly shows that the existing models are not fully capable of modelling flows with strong irrotational rate of strain. We believe that results presented in this study can help to calibrate proposed models

for the rapid pressure–strain term for flows with strong rate of strain and, thus, spatial inhomogeneity.

We acknowledge partial support from US Department of Energy Grants DE-FC36-99GD16416 and DE-FC36-02ID14267.

REFERENCES

Alvelius, K. 1999 Random forcing of three dimensional homogeneous turbulence. *Phys. Fluids* **11**, 1880.

Batchelor, G. & Proudman, I. 1954 The effect of rapid distortion of a fluid in turbulent motion. *Q. J. Mech. Appl. Maths* **7**, 83.

Brown, M. L. 2005 Dynamics of rigid fibers in a planar converging channel. PhD thesis, Georgia Institute of Technology, Atlanta.

Burattini, P., Lavoie, P. & Antonia, R. A. 2005 On the normalized turbulent dissipation rate. *Phys. Fluid* **17**, 098103-1.

Choi, K. S. & Lumley, J. L. 2001 The return to isotropy of homogeneous turbulence. *J. Fluid Mech.* **436**, 59.

Comte-Bellot, G. & Corrsin, S. 1966 The use of a contraction to improve the isotropy of grid generated turbulence. *J. Fluid Mech.* **25**, 657.

Frenkiel, F. N. 1948 The decay of isotropic turbulence. *Trans. ASME: J. Appl. Mech.* 311.

Gence, J. N. & Mathieu, J. 1979 On the application of successive plane strains to grid-generated turbulence. *J. Fluid Mech.* **93**, 501.

Gence, J. N. & Mathieu, J. 1980 The return to isotropy of an homogeneous turbulence having been submitted to two successive plane strains. *J. Fluid Mech.* **101**, 555.

Hussain, A. & Ramjee, V. 1976 Effects of the axisymmetric contraction shape on incompressible turbulent flow. *J. Fluids Engng* **98**, 58.

Launder, B. E., Reece, G. J. & Rodi, W. 1975 Progress in the development of a Reynolds-stress turbulence closure. *J. Fluid Mech.* **41**, 537.

Lumley, J. L. 1970 *Stochastic Tools in Turbulence*. Academic.

Lumley, J. L. 1978 Computational modeling of turbulent flows. In *Advances in Applied Mechanics*, vol. 18, pp. 123–175. Academic.

Lumley, J. L. & Newman, G. R. 1977 The return to isotropy of homogeneous turbulence. *J. Fluid Mech.* **82**, 161.

Mydlarski, L. & Warhaft, Z. 1996 On the onset of high-Reynolds-number grid-generated wind tunnel turbulence. *J. Fluid Mech.* **320**, 331.

Nobach, H., Müller, E. & Tropea, C. 1998 Efficient estimation of power spectral density from laser Doppler anemometer data. *Exps. Fluids*, **24**, 499.

Parsheh, M., Brown, M. L. & Aidun, C. K. 2005 On the orientation of stiff fibres suspended in turbulent flow in a planar contraction. *J. Fluid Mech.* **545**, 245.

Prandtl, L. 1933 Attaining steady air stream in wind tunnels. *NACA Rep.* 726.

Ramjee, V. & Hussain, A. 1976 Influence of axisymmetric contraction on free-stream turbulence. *J. Fluids Engng* **98**, 506.

Ribner, H. & Tucker, M. 1953 Spectrum of turbulence in a contracting stream. *NACA Rep.* 1113.

Roach, P. 1987 The generation of nearly isotropic turbulence by means of grids. *Heat Fluid Flow* **8**, 82.

Sirivat, A. & Warhaft, Z. 1983 The effect of a passive cross-stream temperature gradient on the evolution temperature variance and heat flux in grid turbulence. *J. Fluid Mech.* **128**, 323.

Sjögren, T. & Johansson, A. V. 1998 Measurement and modelling of homogeneous axisymmetric turbulence. *J. Fluid Mech.* **374**, 59.

Taylor, G. I. 1935 Turbulence in a contracting stream. *Z. Angew. Math. Mech.* **15**, 91.

Tsuge, S. 1984 Effect of flow contraction on evolution of turbulence. *Phy. Fluids* **27**, 1948.

Tucker, H. J. & Reynolds, A. J. 1968 The distortion of turbulence by irrotational plane strain. *J. Fluid Mech.* **32**, 567.

Uberoi, M. 1956 Effect of wind tunnel contraction on free stream turbulence. *J. Aero. Sci.* **23**, 756.

Warhaft, Z. 1980 An experimental study of the effect of uniform strain on thermal fluctuations in grid generated turbulence. *J. Fluid Mech.* **99**, 545.